Jour. Fac. Sci., Hokkaido Univ., Ser. VII (Geophysics), Vol. 11, No. 2, 479-499, 1998.

Modeling of a Thermohaline Process with the Theory of Potential Vorticity Homogenization

Shigeto Nishino and Shoshiro Minobe

Division of Earth and Planetary Science, Graduate School of Science, Hokkaido University, Sapporo 060-0810, Japan

(Received November 30, 1997)

Abstract

In order to provide a new perspective for the circulation mechanism of the mid-depth water, an analytical model is constructed so as to include a thermohaline process into the wind-driven theory proposed by Rhines and Young (1982 a, b). The model has three and a half layers, in which the second and third layers correspond to the mid-depth. The wind forcing is formulated as the Ekman pumping at the top of the first layer. The thermohaline forcing is taken into account as diapycnal flows at the upper and lower interfaces of each layer. The diapycnal velocity is obtained from density stratification which is represented by layer thicknesses. In the present model, the layer thicknesses are approximated to those obtained by the wind-driven theory. This approximation allows us to linearize the potential vorticity equation of the geostrophic motion. Integrating the potential vorticity equation, a flow field is obtained outside a region where the potential vorticity is homogeneous. The resultant flow field in the third layer indicates a distinct difference to the result of Rhines and Young (1982 a, b). In this layer, in addition to the wind-driven gyre, divergence of diapycnal flow causes eastward currents to the south of a region where the second layer potential vorticity is homogeneous. The eastward currents have its maximum velocity along the southern edge of the potential vorticity homogenized region of the second layer.

1. Introduction

In order to understand the mechanism of the mid-depth water circulation, one must consider the influences of both the wind and thermohaline forcings, which play dominant roles in the upper and deep oceans, respectively. Most theories of the ocean circulation have taken account of either the wind-driven circulation or the thermohaline circulation. The wind-driven circulation is mainly examined in the upper ocean which is directly ventilated by the wind. In the mid-depth, Rhines and Young (1982 a, b; hereafter referred to as RY) proposed a theory for the wind-driven circulation which is driven not by the direct wind forcing but by the vertical friction due to mesoscale eddies. In their

theory, the wind-driven circulation exists in the region where the potential vorticity (PV) has a uniform value. For an abbreviation, the region is referred to as the PV homogenized region. On the other hand, the circulation in the deep ocean has been studied as a context of the thermohaline circulation (Stommel and Arons, 1960 a, b).

The combined effects of the two forcings for the ocean circulation have been examined theoretically by some researchers (Veronis, 1978; Luyten and Stommel, 1986; Pedlosky, 1986; Tziperman, 1986; Cushman-Roisin, 1987; de Szoeke, 1995). Most of them studied two-layer models with equations written in a characteistic coordinate defined by the barotropic velocity and the first baroclinic Rossby wave. Although the introduction of the characteristic coordinate sheds light on the physics, vertical resolutions of the models are too low to understand the mechanism of the mid-depth water circulation. Assuming the thermohaline forcing is much smaller than the wind forcing, Pedlosky (1986) and Tziperman (1986) analyzed models that have more than two layers. However, those models are modified LPS model (Luyten et al., 1983). The thermohaline effect combined with the RY theory has not been examined so far. In order to understand the mid-depth water circulation, it is necessary to have a theoretical frame work for the circulation which is driven by the thermohaline forcing and the vertical friction due to mesoscale eddies based on the RY theory.

The relative importance of the wind and thermohaline forcings for the mid-depth water circulation is different among the oceans. In the North Pacific, waters in the mid-depth do not outcrop at the sea surface of the basin. Therefore, the wind forcing does not drive the waters directly. However, through the vertical friction proposed by RY, the momentum given by the wind is transported from the upper ocean to the mid-depth ocean. In addition, the thermohaline forcing is caused by the diapycnal fluxes of inputted waters from the other basins such as the Okhotsk Sea (Talley, 1991) and the South Pacific (Reid, 1965; Mantyla and Reid, 1983) under the advective-diffusive density balance. A strong thermohaline forcing caused by the deep convection due to a strong local cooling is not seen in the mid-depth of the North Pacific. On the other hand, the mid-depth of the North Atlantic is affected by Subpolar Mode Water and Labrador Sea Water which are formed at the sea surface of the basin. As a result, the waters are forced by the direct wind forcing and the strong local coolings at the sea surface. In the present paper, a theoretical model is proposed, which explains the mid-depth water circulation without outcropping. The present model is, therefore, suitable for the North Pacific Ocean.

In the subtropical North Pacific, water masses can be classified into following four layers : a surface layer ; an upper intermediate layer ; a lower intermediate layer ; and a deep layer. Only the surface layer outcrops at the sea surface, and directly forced by the wind. All the other layers below the surface layer do not outcrop. The upper intermediate layer contains North Pacific Intermediate Water (NPIW) which is characterized by a salinity minimum (Sverdrup et al., 1942 ; Reid, 1965). The lower intermediate layer is characterized by an oxygen minimum. In this layer, accompanying with degeneration of a salinity minimum, Antarctic Intermediate Water (AAIW) from the South Pacific flows into the region south of the oxygen minimum in the North Pacific (Reid, 1965 ; Reid and Mantyla, 1978). The deep layer consists of North Pacific Deep Water (NPDW) and Lower Circumpolar Water (LCPW) which are discussed by Reid and Lynn (1971), Mantyla (1975) and Mantyla and Reid (1983).

In the above four layers, the RY theory can be applicable to the upper and lower intermediate layers. According to a theoretical study of Rhines and Holland (1979), the momentum inputted by the wind forcing at the sea surface is transferred into the intermediate layers by means of a mesoscale eddy activity as a form of vertical stress, which arises from the baroclinic instability associated with mean circulation, and hence the stress is refereed to as mesoscale eddy stress. Rhines and Young (1982 b) suggested that the mesoscale eddy stress acts to diffuse the potential vorticity horizontally, and in the region of a closed stream line the potential vorticity is homogenized through the horizontal diffusion. As a consequence, motion can occur in the PV homogenized region in the intermediate layers. The region is restricted to the northwestern corner of the subtropical ocean, and its area decreases as the depth increases.

Observational studies, however, have suggested the existence of oceanic currents even outside the PV homogenized region in the lower intermediate layer. In this layer, the homogenized region contracts to the north of 30°N, and the region is much smaller than that in the upper intermediate layer. Using hydrographic data, geostrophic flow fields near the depth of 1000 m, which corresponds to the lower intermediate layer, were estimated by Reid (1965), Reid and Arthur (1975), and Reid and Mantyla (1978). As suggested by the theoretical study of RY, the resultant current fields are characterized by an anticyclonic gyre within the PV homogenized region in the latitudinal range between 30°N and 45°N. However, outside the homogenized region, a broad eastward flow to the south of the anticyclonic gyre appears in the results of Reid (1965) and Reid and Arthur (1975), or another anticyclonic gyre appears between 15°N and 25°N in the result of Reid and Mantyla (1978). In addition, recent float observations by

U. S. World Ocean Circulation Experiment (WOCE) program in the region of 20°N-45°N and 140°E-180° showed the eastward flow which appears between 20°N and 30°N (see Fig. 2, Fig. 3 of Riser, 1995).

The currents to the south of the anticyclonic gyre of 30°N-45°N are in the region where the meridional gradient of potential vorticity is large (see Fig. 4 of Talley, 1988). If the potential vorticity of a water parcel is conserved, a flow is only possible along a zonal contour of potential vorticity which eventually encounters the eastern boundary. However, applying a no-normal flow condition at the eastern boundary, the zonal flow does not occur. Therefore, in the case where any flows exist in the region of the steep meridional gradient of potential vorticity, the potential vorticity cannot be conserved.

In order to explain the flow which intersects the potential vorticity contours outside the PV homogenized region, an additional forcing besides the mesoscale eddy stress is required. An agent for the change of potential vorticity along the current path is vertical stretching (compressing) of a water column associated with the divergence (convergence) of diapycnal flow caused by a thermohaline process. From the conservation equation of density, a density flux due to the diapycnal flow must be balanced, in a steady state, by a density flux caused by the diffusion normal to a density surface. Based on the equation, the diapycnal velocity can be obtained from the density stratification which is represented by layer thicknesses in a layer model.

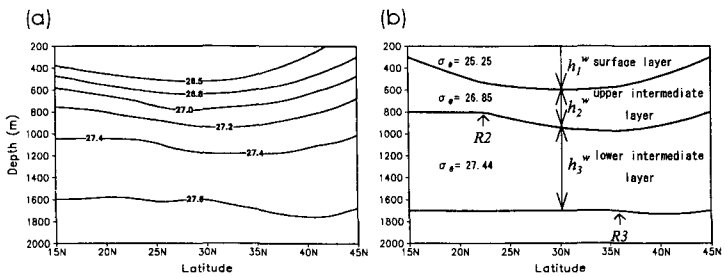

Fig. 1. Meridional cross sections of (a) observed density surfaces along the dateline, and (b) modeled layer interfaces at an equivalent location to the dateline. The distance from the location to the eastern boundary is take to be equivalent to the distance between the dateline and the North American coast. The observed density distribution is based on the datasets of Levitus and Boyer (1994). The model was proposed by Pedlosky and Young (1983). Details of the model description are given in Section 2.1, in terms of the layer thicknesses of h_1^w, h_2^w, and h_3^w. In (a), contours in the surface layer less than 26.5 σ_θ are omitted to avoid crowdedness. In (b), R2 (R3) represents a position of a southern boundary of the potential vorticity homogenized region in the upper (lower) intermediate layer.

The density stratification in the North Pacific is approximately explained by the RY theory. The distribution of the observed PV homogenized region shown by Talley (1988) agrees well to that expected from the model proposed by Pedlosky and Young (1983 ; hereafter referred to as PY), which is based on RY theory. Furthermore, the similarity between the observed stratification in the North Pacific and the layer thicknesses given by the PY model is evident as shown in Fig. 1. This suggests that the density stratification for determining the diapycnal velocity can be obtained by using the PY model as a good approximation.

Combining the thermohaline process with the PY model, a new model for the mid-depth water circulation is constructed in the present paper. By employing the approximation of the density stratification with the PY model, it allows us to obtain an analytical solution of the total current field caused by the wind and thermohaline forcings. The detailed solution of the model is described in Section 2 and the results are depicted in Section 3. Section 4 is a discussion throughout the present study. The main conclusions are presented in Section 5.

2. Analytical model

2.1 Governing equations and solution

The model basin is idealized as rectangular and divided into four vertical layers : the surface layer, the upper intermediate layer, the lower intermediate

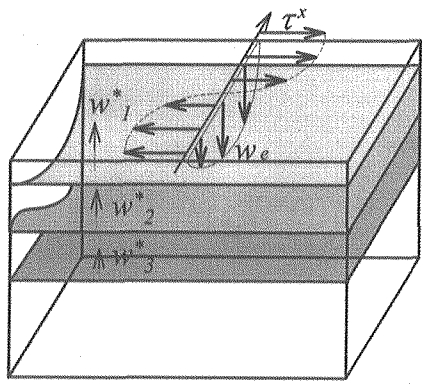

Fig. 2. Schematic of the three and a half layers model. The Ekman pumping, w_e, is given by the curl of the wind stress, τ^x. The diapycnal flows, w_1^*, w_2^*, and w_3^*, are taken into account as the forcing accompanied by a thermohaline process.

layer, and the deep layer. The deep layer is assumed to be at rest with infinite depth. The present model has only the interior region of the ocean, excluding the western boundary region. The wind forcing is formulated as the Ekman pumping at the top of the surface layer. The thermohaline forcing is taken into account as the diapycnal flows at the upper and lower interfaces of each layer. The motion in each layer is assumed to be geostrophic and hydrostatic, and the fluid satisfies continuity. A schematic feature of the model is shown in Fig. 2.

The present model is solved as following two steps: in the first step, the layer thickness accompanied by the wind-driven circulation is calculated by using the PY model; in the second step, the deviation of layer thickness due to the thermohaline effect from the thickness of the wind-driven circulation is obtained. The velocity of the wind-driven circulation and the accompanying layer thickness in the nth layer are denoted as (u_n^w, v_n^w), and h_n^w, respectively. On the other hand, the deviations of velocity and layer thickness due to the thermohaline effect are indicated as (u_n^d, v_n^d), and h_n^d, respectively.

The wind-driven circulation and the accompanying layer thickness are determined as follows. Two conditions are employed: one is a no normal-flow condition at the eastern boundary ($x=x_E$), and the other is a no cross-flow condition at the northern boundary ($f=f_N$), where x is the zonal distance from the western boundary and f is the Coriolis parameter, respectively. Based on these conditions, the layer thickness at the eastern boundary is the same as that at the northern boundary, which is expressed as H_n. Furthermore, according to the RY theory, potential vorticity is assumed to be constant in which the anticyclonic gyre appears in the second and third layers (the upper and lower intermediate layers). Consequently, the constant value of potential vorticity in the nth layer is determined by the layer thickness at the eastern and northern boundaries, H_n:

$$\frac{f}{h_n^w}=\frac{f_N}{H_n}=\text{constant} \qquad (n=2,3). \tag{1}$$

In addition, the Sverdrup balance holds from the first layer to the mth layer which are in motion:

$$\beta\sum_{n=1}^{m} v_n^w h_n^w = f w_e, \tag{2}$$

where w_e is the Ekman pumping velocity. Assuming the density in each layer as ρ_n, and using the geostrophic relation, the meridional velocity of the wind-driven circulation is given by

$$v_n^w=\sum_{j=n}^{3}\frac{\gamma_j}{f}\frac{\partial}{\partial x}\sum_{i=1}^{j}h_i^w, \tag{3}$$

where γ_n is the reduced gravity defined as

$$\gamma_n=-g\frac{\rho_n-\rho_{n+1}}{\rho_0}. \tag{4}$$

Substituting (3) into (2), the Sverdrup balance is expressed as the zonal derivative of layer thickness. Then, integration of (2) starting at the eastern boundary toward the west gives

$$\sum_{n=1}^{m}\gamma_n\left(\sum_{i=1}^{n}h_i^w\right)^2=\sum_{n=1}^{m}\gamma_n\left(\sum_{i=1}^{n}H_i\right)^2+\gamma_1 D_0^2 \tag{5}$$

where D_0^2 is given by

$$D_0^2=-\frac{2f^2}{\gamma_1\beta}\int_x^{x_E}w_e dx. \tag{6}$$

The layer thickness of the wind-driven circulation is obtained by solving (1) and (5). From the layer thickness, the velocity field of the wind-driven circulation is determined by using the geostrophic relation:

$$\begin{cases} u_n^w=-\sum_{j=n}^{3}\frac{\gamma_j}{f}\frac{\partial}{\partial y}\sum_{i=1}^{j}h_i^w, \\ v_n^w=\sum_{j=n}^{3}\frac{\gamma_j}{f}\frac{\partial}{\partial x}\sum_{i=1}^{j}h_i^w. \end{cases} \tag{7}$$

In addition to the wind-driven circulation, the thermohaline effect induces the motion. The diapycnal flow causes input of potential vorticity and gives rise to the circulation which accompanies the deviation of layer thickness from that determined by the wind-driven circulation. Hereafter, for the simplicity, this additional circulation to the wind-driven circulation is referred to as thermohaline-forced circulation. Although the thermohaline-forced circulation is driven by the diapycnal flow that is associated with the thermohaline process of the advective-diffusive density balance, the circulation is not solely caused by the thermohaline process. As described in the previous section, the distribution of the diapycnal flow depends on the density stratification which is approximately determined by the wind-driven circulation. Therefore, the thermohaline-forced circulation is also affected by the wind forcing.

As shown by Tziperman (1986), Huang and Bryan (1987) and Yin et al. (1992), the diapycnal flow, w_n^*, can be expressed as follows.

$$w_n^*=k^*\frac{\Delta_n\rho/(h_n^w+h_n^d)-\Delta_{n+1}\rho/(h_{n+1}^w+h_{n+1}^d)}{\rho_n-\rho_{n+1}} \tag{8}$$

where k^* is the diffusion coefficient of the diapycnal mixing, and $\Delta_n\rho$ is the density difference between the top and bottom of the nth layer. If the densities at the top and bottom of the nth layer are represented as ρ_n^u and ρ_n^l respectively, the density difference is defined as $\Delta_n\rho \equiv \rho_n^u - \rho_n^l$. The density at the bottom of the nth layer is the same as the density at the top of the $n+1$th layer. The assumption that the density stratification can be approximated to that determined by the wind-driven circulation is valid, if $h_n^w >> h_n^d$. The good agreement in the density stratification between the observation and the PY model shown in Fig. 1 suggests that this relation well holds. In this case, (8) is approximated as

$$w_n^* = k^* \frac{\Delta_n\rho/h_n^w - \Delta_{n+1}\rho/h_{n+1}^w}{\rho_n - \rho_{n+1}} \tag{9}$$

Consequently, the diapycnal flow depends on the layer thicknesses that are determined by the PY model, with the prescribed layer densities and density differences.

The deviation of layer thickness, h_n^d, accompanied by the thermohaline-forced circulation is calculated from the potential vorticity balance. Under the relation, $h_n^w >> h_n^d$, potential vorticity equation outside the PV homogenized region becomes

$$u_n^d \frac{\partial}{\partial x}\left(\frac{f}{h_n^w}\right) + v_n^d \frac{\partial}{\partial y}\left(\frac{f}{h_n^w}\right) = \frac{f(w_{n-1}^* - w_n^*)}{h_n^{w2}}, \tag{10}$$

$$\begin{cases} u_n^d = -\sum_{j=n}^{3} \frac{\gamma_j}{f} \frac{\partial}{\partial y} \sum_{i=1}^{j} h_i^d, \\ v_n^d = \sum_{j=n}^{3} \frac{\gamma_j}{f} \frac{\partial}{\partial x} \sum_{i=1}^{j} h_i^d. \end{cases} \tag{11}$$

In the lower intermediate layer ($n=3$), the potential vorticity equation of (10) is written as

$$\frac{\partial}{\partial y}\left(\frac{f}{h_3^w}\right)\frac{\partial d_3^d}{\partial x} - \frac{\partial}{\partial x}\left(\frac{f}{h_3^w}\right)\frac{\partial d_3^d}{\partial y} = \frac{1}{\gamma_3}\left(\frac{f}{h_3^w}\right)^2 (w_2^* - w_3^*), \tag{12}$$

where $d_3^d = h_1^d + h_2^d + h_3^d$ is the summation of layer thickness deviations or the distortion of the density surface at the bottom of the lower intermediate layer. The solution of d_3^d is obtained by integrating the right hand side of (12) along a characteristic path, f/h_3^w=constant, from the eastern boundary where d_3^d is presumed to be zero. Subsequently, the velocity field of the thermohaline-forced circulation can be calculated from (11). Likewise, the velocity field in the upper intermediate layer is evaluated from the distributions of the divergence of diapycnal flow, $w_1^* - w_2^*$, along the characteristic path, f/h_2^w=constant.

2.2 Parameters

Model parameters are chosen to be suitable for the North Pacific Ocean. The modeled region is the subtropical ocean from 15°N to 45°N meridionally, and 80° width zonally. The Ekman pumping at the upper surface is given as

$$w_e = -\frac{1}{\rho_0 f}\left(\frac{\partial \tau^x}{\partial y}\right), \tag{13}$$

$$\tau^x = -A\cos\frac{\pi(\theta-\theta_s)}{L_y}, \tag{14}$$

where τ^x is the zonal component of the wind stress, θ is the latitude, θ_s denotes the latitude of the southern boundary, and L_y is the meridional length scale of the model ocean, A is the amplitude of the wind stress, which is set as 0.1 N m^{-2}.

The density at the interfaces of the layers and the density of each layer are chosen as follows. As described in the previous subsection, the density at the interfaces are used for the calculation of the diapycnal velocity. The density at the model surface, that is, the upper interface of the first layer, is given by a linear interpolation from 22.5 σ_θ at 15°N to 25.5 σ_θ at 45°N. The lower interface density of the first layer is determined from the densest outcropping density in the North Pacific. Although the 26.7 σ_θ surface outcrops to narrow regions near northern Honshu and Hokkaido, Japan in winter (Talley and Nagata, 1991; Talley, 1993), the 26.5 σ_θ surface approximately corresponds to the densest water that outcrops to a relatively broad region in the open ocean (Roemmich et al., 1991; Keffer, 1985). Therefore, most of the waters denser than 26.5 σ_θ do not expose to the direct wind forcing. The density at the lower interface of the first layer is set as 26.5 σ_θ. The upper intermediate layer which contains NPIW lies in a density range from 26.5 σ_θ to 27.2 σ_θ. It is confirmed from the oxygen distribution based on Levitus' (1982) climatology that the density surfaces deeper than 27.2 σ_θ are affected by a different water mass originated from AAIW. The density at the interface between the upper and lower intermediate layers is chosen as 27.2 σ_θ. The water mass traced to AAIW is observed from 800 m to 2000 m along 24°N (Bryden et al., 1991), with the corresponding density range from 27.2 σ_θ to 27.67 σ_θ. Therefore, we set the density of the lower interface of the lower intermediate layer as 27.67 σ_θ. The density of the first three layers are given by 25.25, 26.85, and 27.44 σ_θ, respectively. These values are approximately the same as the averaged values of the density at the upper and lower interfaces. The density of the fourth layer is chosen as 27.73 σ_θ, which is about the averaged density of NPDW

The other model parameters are as follows. The layer thicknesses at the eastern boundary are $H_1=300$ m, $H_2=500$ m, and $H_3=900$ m, respectively. The diffusion coefficient is given as $k^*=5\times10^{-5}$ m^2 s^{-1}. The diapycnal flow from the deep layer is assumed to be constant as $w_3^*=7.7\times10^{-8}$ m s^{-1}. This value is obtained from (9), assuming the lower interface of NPDW to be 27.78 σ_θ at 3200 m. Using these parameters, the divergences in the surface, upper intermediate, and lower intermediate layers, which are identical to the amounts of inflows into the model region through the western, southern, and northern boundaries, become -3.4, 0.93, and 0.59 Sv, respectively.

3. Results

The velocity fields in the upper and lower intermediate layers obtained from the model are shown in Figs. 3(a) and 3(b), respectively. In the figures, the curves of R2 and R3 represent southern boundaries of the PV homogenized region in the upper and lower intermediate layers, respectively. In the homogenized region, the velocity field is calculated from (7). As is the case with the PY model, the anticyclonic wind-driven gyre exists in this region. In addition, the circulation arises outside the homogenized region. This flow is newly obtained in the present model due to the diapycnal flow. It is noteworthy that eastward flow appears in the lower intermediate layer to the south of the R2 curve, and the current velocity has its maximum along the curve.

The thermohaline forcing in the lower intermediate layer, that is, the divergence of diapycnal flow, $w_2^*-w_3^*$, is indicated in Fig. 4. In this figure, the maximum divergence of diapycnal flow is found along the R2 curve. This suggests that the outflow velocity at the top of the lower intermediate layer, w_2^*, has its maximum along the R2 curve, because the inflow velocity at the bottom of the lower intermediate layer, w_3^*, is constant. The diapycnal velocity is calculated from (9). The velocity at the top of the lower intermediate layer depends only on the layer thickness, because the density in each layer and the density differences between the top and bottom of the upper and lower intermediate layers are constant. From the meridional section of layer thickness shown in Fig. 1(b), it is suggested that the layer thickness of the upper intermediate layer has the minimum at the position of R2, and it is the same position that the layer thickness of the lower intermediate layer has its maximum. Therefore, the upward velocity at the top of the lower intermediate layer becomes maximum at this position, R2.

The distortion of the bottom density surface of the lower intermediate

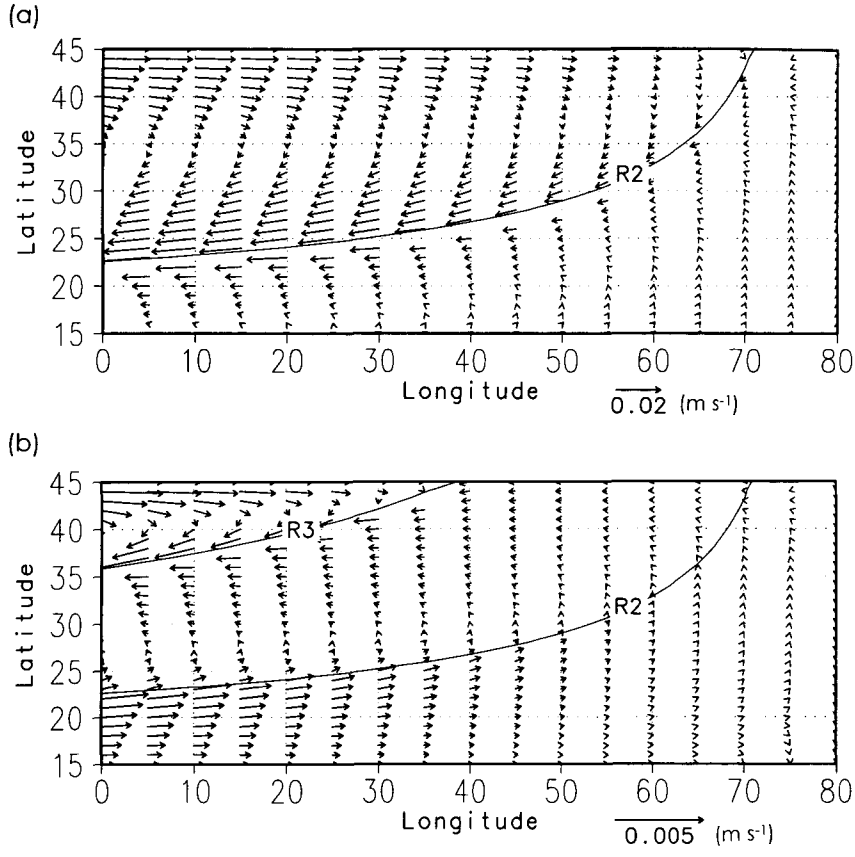

Fig. 3. Velocity fields obtained from the model (a) in the upper intermediate layer and (b) in the lower intermediate layer. In the region to the northwest of the curve of R2 (R3), potential vorticity is homogenized in the upper (lower) intermediate layer.

layer, d_3^d, which prescribes the flow field of (u_3^d, v_3^d) is obtained by integrating the right hand side of (12) along the characteristic path, f/h_3^w=constant (Fig. 5), from the eastern boundary. Integrating in this way, the distribution of d_3^d is given as Fig. 6. The characteristic paths emanating from the eastern boundary cannot penetrate further north of the R3 curve where the potential vorticity is uniform. Therefore, the solution of d_3^d cannot exist in this region. Figure 6 indicates that the circulation outside the PV homogenized region is cyclonic centered on the region of the large negative values of d_3^d where the bottom density surface is lifted up. Furthermore, the gradient of the bottom density surface becomes

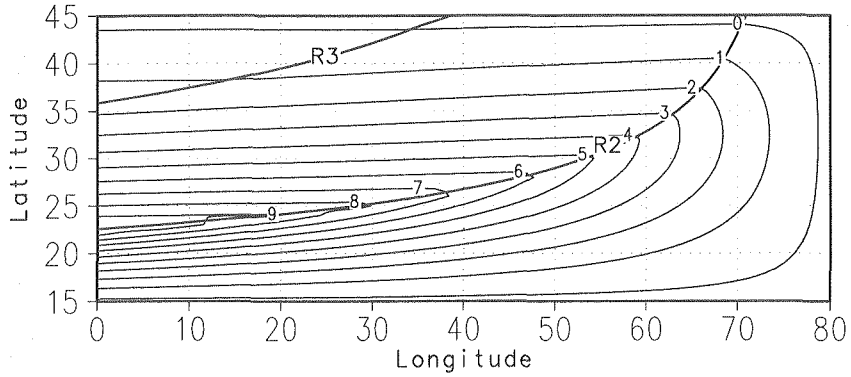

Fig. 4. Difference of diapycnal velocity between the upper and lower interfaces of the lower intermediate layer, $w_2^* - w_3^*$. The unit of the contour label is 10^{-8} m s^{-1}, and the contour interval is 1×10^{-8} m s^{-1}. The two curves, R2 and R3, are the same as those shown in Fig. 3.

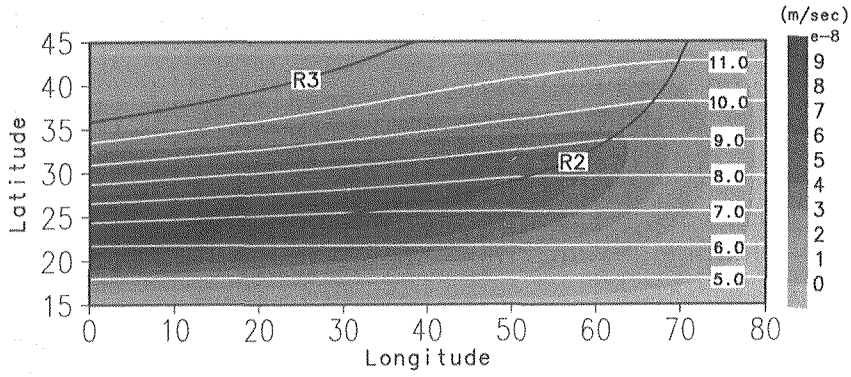

Fig. 5. Characteristic paths (white contours) and divergence of diapycnal flow (shades) in the lower intermediate layer. The characteristic paths are given by f/h_3^w (see (12)). The unit of the contour label is 10^{-8} m^{-1} s^{-1}, and the contour interval is 1×10^{-8} m^{-1} s^{-1}. The divergence of diapycnal flow shown in Fig. 4 is superimposed with shades. Darker (Lighter) shades correspond to larger (smaller) divergence.

large to the south of the R2 curve where the significant eastward flow appears.

In the case where the characteristic path goes through the divergence field of diapycnal flow as shown in Fig. 5, d_3^d becomes small as going to the west along the characteristic path. In other words, the bottom density surface of the lower intermediate layer becomes shallow with the distance on the characteristic path increases from the eastern boundary. This is confirmed by comparing Fig. 5

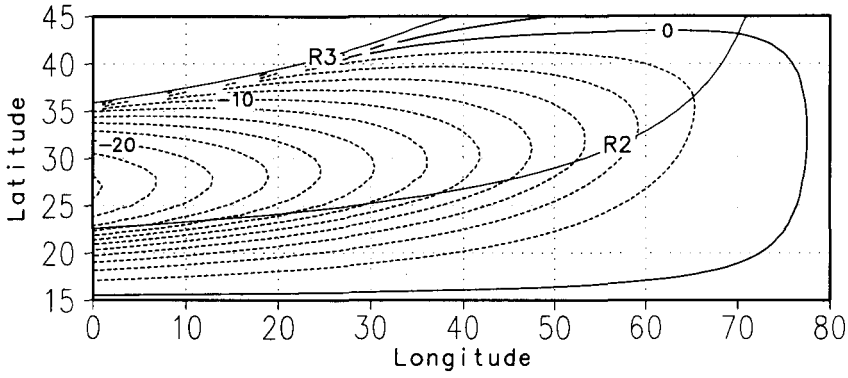

Fig. 6. Depth anomaly of the interface between the lower intermediate layer and the deep layer relative to its depth at the eastern boundary (1700 m). The anomaly is caused by the thermohaline-forced motion. If the thermohaline effect is ignored, the depth anomaly becomes zero.

with Fig. 6. In Fig. 5, the characteristic paths extend almost zonal at regular intervals. Therefore, the meridional difference in the integration of the right hand side of (12) along the characteristic path gives rise to the meridional gradient of the bottom density surface, $\partial d_3^g/\partial y$, which provides the zonal component of the geostrophic flow, u_3^g. The right hand side of (12) is a product of the square of potential vorticity on the characteristic path, $(f/h_3^w)^2$, and the divergence of diapycnal flow, $w_2^* - w_3^*$. The former, that is, the potential vorticity in the lower intermediate layer becomes large with increasing latitude between the southern boundary and the R3 curve. The latter, which is the divergence of diapycnal flow, also becomes large with increasing latitude as far as the R2 curve. However, further north of the R2 curve, the divergence of diapycnal flow becomes small with increasing latitude. For this reason, the meridional difference in the right hand side of (12) becomes larger in the southern side of the R2 curve than that in the northern side. Therefore, the gradient of the bottom density surface becomes large to the south of the R2 curve, and the significant eastward flow is induced in this region.

The appearance of the eastward flow to the south of the R2 curve is also explained by the Sverdrup balance and the continuity of the fluid. In the lower intermediate layer, because the layer thickness of the wind-driven circulation is constant to the south of the R2 curve, (12) leads the following Sverdrup relation:

$$\beta v_3^g = f\frac{w_2^* - w_3^*}{H_3}. \tag{15}$$

Furthermore, the continuity equation becomes

$$\frac{\partial u_3^d}{\partial x}+\frac{\partial v_3^d}{\partial y}+\frac{w_2^*-w_3^*}{H_3}=0. \tag{16}$$

Substituting (15) into (16), the divergence of zonal flow is expressed as

$$\frac{\partial u_3}{\partial x}=-2\frac{w_2^*-w_3^*}{H_3}-\frac{f}{\beta H_3}\frac{\partial w_2^*}{\partial y}. \tag{17}$$

In (17), $\partial w_2^*/\partial y>0$ holds to the south of R2. This is indicated from Fig. 4 in which $w_2^*-w_3^*$ becomes large as going to the north between the southern boundary and the R2 curve, while w_3^* is constant. The increment of w_2^* with increasing latitude is attributed to the decrement of the layer thickness of the upper intermediate layer with increasing latitude. Because $\partial w_2^*/\partial y>0$ holds in (17) to the south of R2, $\partial u_3^d/\partial x<0$ is obtained, if only $w_2^*-w_3^*>0$. That is, if the divergence of diapycnal flow occurs in the lower intermediate layer, the flow becomes large in the direction of the east as going to the west.

In addition to the southern side of the R2 curve, another region where the thermohaline-forced circulation forms the relatively significant flow in the lower intermediate layer is just to the south of the R3 curve. The direction of the flow in the latter region depends on a sign of $w_2^*-w_3^*$ near a point where the R3 curve intersects the northern boundary of the model. The point of intersection is called as a Rossby repeller. At this point, the meridional gradient of potential vorticity is zero and the propagation speed in an advection equation of d_3^d, (12), which is defined by the potential vorticity gradient is infinitesimal. Because the thermohaline forcing is accumulated along the characteristic path, the accumulation rate becomes large as the propagation speed decreases. Therefore, near the Rossby repeller, the thermohaline forcing is accumulated too much along the characteristic path, since the propagation speed slows down there. Consequently, if $w_2^*-w_3^*<0$ ($w_2^*-w_3^*>0$) near the Rossby repeller, d_3^d becomes large (small) drastically as one goes to the southwest along the characteristic path. Because the characteristic paths which extend with the different propagation speed near the Rossby repeller come close to each other as going to the west in the region just to the south of the R3 curve, the meridional gradient of d_3^d becomes large, and relatively significant flow appears. In the case of $w_2^*-w_3^*<0$ ($w_2^*-w_3^*>0$) near the Rossby repeller, d_3^d becomes large (small) with increasing latitude, and westward (eastward) flow appears just to the south of the R3 curve. However, the fact that the propagation speed along the characteristic path is extremely slow near the Rossby repeller might derive the importance of other process such as diffusion, resulting in that the steepness of d_3^d would be smoothed. There-

fore, the frontal flow just to the south of the R3 curve in the model is expected to be weaken in the real ocean. Moreover, it is suggested from the oxygen distribution that the direction of the flow just to the south of the R3 curve would be westward as shown in Fig. 3(b). This point is discussed more in detail in the next section.

4. Discussion

The existence of the eastward flow in the lower intermediate layer to the south of the R2 curve in the present model agrees well with the aforementioned results of the geostrophic calculations (Reid, 1965 ; Reid and Arthur, 1975 ; Reid and Mantyla, 1978) and the direct measurements of the flow field (Riser, 1995). Reid and Mantyla (1978), however, indicated a circulation pattern different from that obtained from the model and other geostrophic calculations. In their result (see Fig. 4 of Reid and Mantyla, 1978), the eastward flow returns to the west forming an anticyclonic gyre. However, the corresponding westward flow cannot be seen in the results of the model and other geostrophic calculations.

For the formation of the westward flow in the lower intermediate layer to the south of the R2 curve, model parameters should be set so that the convergence of diapycnal flow occurs in this region, and the convergence effect expressed in the first term of the right hand side in (17) must be larger than the influence of meridional gradient of w_2^* indicated in the second term. That is, if $\partial u_3^d/\partial x > 0$ holds in (17), the flow becomes large in the direction of west as the longitude decreases. For example, consider the case where w_3^* is 1.4×10^{-7}

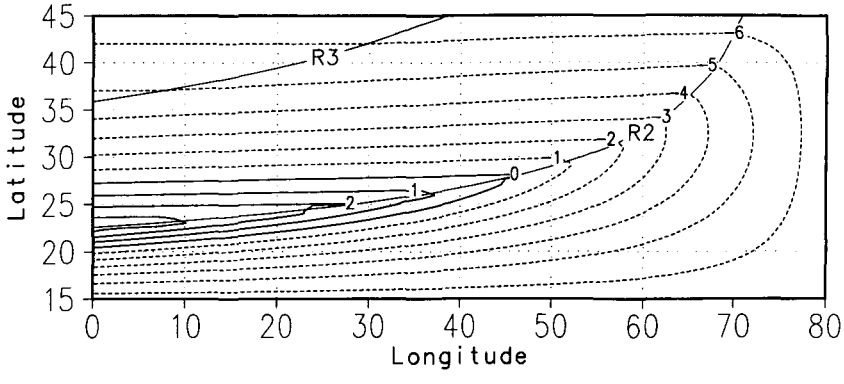

Fig. 7. Same as Fig. 4, except for that the prescribed diapycnal velocity is set to 1.4×10^{-7} m s^{-1} at the interface between the lower intermediate and deep layers.

m s^{-1} which is about twice as large as the value described in Section 2.2, and other parameters are given as the same values. In this case, the distribution of the thermohaline forcing is shown in Fig. 7. In the figure, the convergence occurs except for the limited region along the R2 curve where w_2^* takes the maximum value.

The circulation to the south of the R2 curve driven by the forcing given in Fig. 7 is shown in Fig. 8 in which an anticyclonic gyre can be seen. As described above, in the region where the westward flow develops, the term of the convergence of diapycnal flow in (17) is much larger than the term of the meridional gradient of w_2^*. Figure 7 indicates that the convergence becomes large with decreasing latitude, and the meridional gradient of w_2^* becomes small with increasing longitude further south of the R2 curve. Therefore, the development of the westward flow can be seen in the southeastern region of the model ocean as shown in Fig. 8. On the other hand, in the western region south of the R2 curve, the meridional gradient of w_2^* is larger and the convergence is smaller than those in the east, and weak divergence occurs near the R2 curve (Fig. 7). Consequently, $\partial u_3^g/\partial x$ in (17) becomes negative, and the westward flow disappears in the western region (Fig. 8). As a result, the westward flow appears in the middle longitude near the southern boundary of the model ocean.

Although the circulation pattern in Fig. 8 in which the westward flow appears to the south of the R2 curve is consistent with the geostrophic calculation of Reid and Mantyla (1978), the flow further north of the R2 curve, which

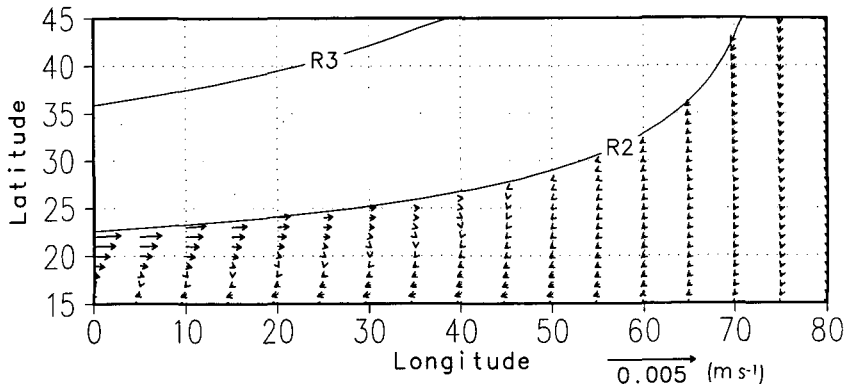

Fig. 8. Same as Fig. 3(b), except for that the prescribed diapycnal velocity is set to 1.4×10^{-7} m s^{-1} at the interface between the lower intermediate and deep layers. The velocity vectors to the northwest of the curve of R2 are not shown, because the magnitude of the vectors is extremely large.

is not shown in Fig. 8, becomes extremely large and the circulation all over the model ocean is unrealistic. That is, it is hard to obtain the westward flow from the present model under the realistic parameter range such as described in Section 2.2. The difficulty of the appearance of the westward flow might be caused by some problems of the model. For example, an uncertain estimation of diapycnal velocity, the assumption of no motion in the deep layer, and the Sverdrup balance assumption to the moving layers. The uncertainty in the estimation of diapycnal velocity is the postulation of constant diffusivity of diapycnal mixing. At the present, it is difficult to give a realistic distribution of the diffusivity. The remaining problems for the no motion in the deep layer and the Sverdrup balance are necessarily to obtain a simple analytical solution of the flow field. If the assumptions of constant diffusivity, no motion in the deep layer, and the Sverdrup balance are relaxed, it might be possible to be seen the westward flow to the south of the R2 curve under the realistic parameter range.

Besides the thermohaline effect, other possible agent to drive the motion outside the PV homogenized region is the eddy stress that transports momentum from the surface layer to the lower layers. Rhines and Holland (1979) suggested that the eddy stress is caused by the eddy flux of potential vorticity and the eddy flux is related to the mean gradient of potential vorticity by means of eddy diffusion. As shown in Fig. 5, the gradient of potential vorticity is large just to the south of the PV homogenized region. Therefore, the eddy stress might be large in this region in spite of the small eddy diffusivity compare to that in the PV homogenized region.

The appearance of the relatively large eddy stress just to the south of the PV homogenized region is confirmed by an eddy-resolving numerical experiment (Holland and Rhines, 1980) of antisymmetric double gyres forced by the wind. In the second layer of the numerical model, the dominant eddy stress occurs near a boundary of the PV homogenized region. As a result, two intense gyres appear, as suggested by the RY theory, in the PV homogenized region with the eastward jet at mid-latitude and westward return flows, and in addition, outside the homogenized region other two weak gyres circulate in the opposite direction to the adjacent intense gyre appearing in the homogenized region. The weak gyres form eastward flows outside the homogenized region. However, the eastward flows are much weaker than the westward return flows, because the eastward flows appear far from the boundary of the PV homogenized region where the dominant eddy stress occurs. Therefore, the circulation driven by the eddy stress does not cause the significant eastward flow in the interior of the basin.

Outside the PV homogenized region in the lower intermediate layer, in addition to the eastward flow, there is another noteworthy flow just to the south of the homogenized region. In the present model, as described in the Section 3, the direction of the flow depends on the sign of $w_2^* - w_3^*$ near the Rossby repeller, and the case of $w_2^* - w_3^* < 0$ is shown in Fig. 3(b). In this case, the direction of the flow just to the south of the PV homogenized region is westward. This westward flow is formed as a result of closeness of the stream lines which are supplied across the northern boundary from the east of the Rossby repeller. Conversely, if $w_2^* - w_3^* > 0$ near the Rossby repeller, the eastward flow appears just to the south of the PV homogenized region. The stream lines of the eastward flow disperse and cross the gyre boundary. In the present model, the frontal flow along the boundary of the PV homogenized region is related to the cross gyre flow. If the direction of the frontal flow is westward, a low oxygen tongue should extend from the east of the gyre boundary to the subtropical region along the boundary of the PV homogenized region. On the other hand, if the direction of the frontal flow is eastward, a high oxygen tongue would extend from the western boundary to the eastern gyre boundary along the boundary of the PV homogenized region. The distribution of oxygen in the North Pacific (see Fig. 3 of Reid and Mantyla, 1978) in which the low oxygen tongue appears along 30°N-35°N supports the existence of the westward frontal flow.

In addition to the divergence of diapycnal flow, the eddy stress would also drive the flow just to the south of the PV homogenized region. In this region, as described above, the gradient of potential vorticity is large and the dominant westward stress should occur compared to those in the interior basin, so the westward flow might be induced as indicated by the numerical experiment of Holland and Rhines (1980). At the present, it is difficult to know which forcing is dominant. In the result of the geostrophic calculation of Reid and Mantyla (1978), the flow just to the south of the PV homogenized region is very week except for the west of 170°E. Therefore, the forcing of the eddy stress which induces the westward flow might be canceled out by the forcing of the divergence of diapycnal flow which causes the eastward flow.

In the present paper, the circulation outside the PV homogenized region in the lower intermediate layer is mainly studied. As a result, it is suggested that the eastward flow in this layer is caused by the divergence of diapycnal flow. However, concerning to the frontal flow, further studies are required to make it clear to understand the interaction of the two forcings, the divergence of diapycnal flow and the eddy stress.

5. Conclusions

In the present study, we have proposed an analytical model, in which both the wind and thermohaline forcings are taken into account, to understand the mechanism of the mid-depth water circulation. The model results exhibit the following features which were not obtained by the previously proposed theory of potential vorticity homogenization.

1. The circulation outside the PV homogenized region is driven by the divergence of diapycnal flow which is accompanied by a thermohaline process.

2. The distributions of diapycnal flow and potential vorticity, which determine the flow field of the thermohaline-forced motion outside the PV homogenized region, are estimated by the layer thicknesses accompanied by the wind-driven circulation. That is, the wind forcing affects the thermohaline-forced motion. Therefore, the circulation outside the homogenized region should be called as the hybrid wind-thermohaline driven circulation.

3. In the third layer, which corresponds to the lower intermediate layer in the North Pacific Ocean, the thermohaline-forced eastward flow appears to the south of the PV homogenized region of the upper layer. The maximum velocity of the eastward flow occurs along the southern boundary of the upper layer homogenized region.

Acknowledgments

The authors would like to express their sincere thanks to Professor Seiichi Kanari for his fruitful discussions and invaluable suggestions. The present paper is a part of a thesis for a doctorate (S. Nishino) submitted to Hokkaido University. Thus, the first author is very grateful to him for his continuous encouragement and useful comments throughout entire graduate career. Moreover, their sincere gratitude is expressed to Dr. Toshiyuki Hibiya of University of Tokyo and Dr. Hirohiko Nakamura of Kagoshima University for their pleasant discussions and encouragements. They also wish to acknowledge to members of Physical Oceanography Laboratory of Hokkaido University for their instructive comments and unforgettable supports.

References

Bryden, H.L., D.H. Roemmich and J.A. Church, 1991. Ocean heat transport across 24°N in the Pacific. Deep-Sea Res., **38**, 297-324.

Cushman-Roisin, B., 1987. On the role of heat flux in the Gulf Stream-Sargasso Sea Subtropical Gyre System. J. Phys. Oceanogr., **17**, 2189-2202.
de Szoeke, R.A., 1995. A model of wind- and buoyancy-driven ocean circulation. J. Phys. Oceanogr., **25**, 918-941.
Holland, W.R. and P.B. Rhines, 1980. An example of eddy induced circulation. J. Phys. Oceanogr., **10**, 1010-1031.
Huang, R.X., and K. Bryan, 1987. A multilayer model of the thermohaline and wind-driven ocean circulation. J. Phys. Oceanogr., **17**, 1909-1924.
Keffer, T., 1985. The ventilation of the world's oceans: maps of the potential vorticity field. J. Phys. Oceanogr., **15**, 509-523.
Levitus, S., 1982. Climatological Atlas of the World Ocean., NOAA Prof. Paper, **13**, 173 pp.
Levitus, S. and T.P. Boyer, 1994. World Ocean Atlas, 1994., NOAA Atlas Series, **4**, 117 pp.
Luyten, J.R., J. Pedlosky and H. Stommel, 1983. The ventilated thermocline. J. Phys. Oceanogr., **13**, 292-309.
Luyten, J.R. and H. Stommel, 1986. Gyres driven by combined wind and buoyancy flux. J. Phys. Oceanogr., **16**, 1551-1560.
Mantyla, A.W., 1975. On the potential temperature in the abyssal Pacific Ocean. J. Mar. Res., **33**, 341-354.
Mantyla, A.W. and J.L. Reid, 1983. Abyssal characteristics of the World Ocean waters. Deep-Sea Res., **30**, 805-833.
Pedlosky, J., 1986. The buoyancy and wind-driven ventilated thermocline. J. Phys. Oceanogr., **16**, 1077-1087.
Pedlosky, J. and W.R. Young, 1983. Ventilation, potential vorticity homogenization and the structure of the ocean circulation. J. Phys. Oceanogr., **13**, 2020-2037.
Reid, J.L., 1965. Intermediate waters of the Pacific Ocean., Johns Hopkins Press, 85 pp.
Reid, J.L. and R.S. Arthur, 1975. Interpretation of maps of geopotential anomaly for the deep Pacific Ocean. J. Mar. Res., **33**, Suppl., 37-52.
Reid, J.L. and R.J. Lynn, 1971. On the influence of the Norwegian-Greenland and Weddell seas upon the bottom waters of the Indian and Pacific oceans. Deep-Sea Res., **18**, 1063-1088.
Reid, J.L. and A.W. Mantyla, 1978. On the mid-depth circulation of the North Pacific Ocean. J. Phys. Oceanogr., **8**, 946-951.
Rhines, P.B. and W.R. Holland, 1979. A theoretical discussion of eddy-driven mean flows. Dyn. Atmos. Oceans, **3**, 289-325.
Rhines, P.B. and W.R. Young, 1982a. A theory of the wind-driven circulation. I. Mid-ocean gyres. J. Mar. Res., **40**, Suppl., 559-596.
Rhines, P.B. and W.R. Young, 1982b. Homogenization of potential vorticity in planetary gyres. J. Fluid Mech., **122**, 347-367.
Riser, S.C., 1995. Pacific RAFOS floats measure mid-depth flow. WOCE Notes, **7**, 1-6.
Roemmich, D., T. McCallister and J. Swift, 1991. A transpacific hydrographic section along latitude 24°N: the distribution of properties in the subtropical gyre. Deep-Sea Res., **38**, S1-S20.
Stommel, H. and A.B. Arons, 1960a. On the abyssal circulation of the World ocean-I. Stationary planetary flow patterns on a sphere. Deep-Sea Res., **6**, 140-154.
Stommel, H. and A.B. Arons, 1960b. On the abyssal circulation of the World ocean-II. An idealized model of the circulation pattern and amplitude in oceanic basins. Deep-Sea Res., **6**, 217-233.
Sverdrup, H., M.W. Johnson and R.H. Fleming, 1942. The Oceans, Their Physics, Chemistry, and General Biology., Prentice-Hall, 1087 pp.
Talley, L.D., 1988. Potential vorticity distribution in the North Pacific. J. Phys. Oceanogr., **18**, 89-106.

Talley, L.D., 1991. An Okhotsk Sea Water anomaly : implications for ventilation in the North Pacific. Deep-Sea Res., **38**, S171-S190.

Talley, L.D., 1993. Distribution and formation of North Pacific Intermediate Water. J. Phys. Oceanogr., **23**, 517-537.

Talley, L.D. and Y. Nagata, 1991. Oyashio and mixed water regions as a formation area of North Pacific Intermediate Water. Umi to Sora, **67**, 65-74.

Tziperman, E., 1986. On the role of interior mixing and air-sea fluxes in determining the stratification and circulation of the ocean. J. Phys. Oceanogr., **16**, 680-693.

Veronis, G., 1975. Model of world ocean circulation: III. Thermally and wind driven. J. Mar. Res., **36**, 1-44.

Yin, F.L., I.Y. Fung and C.K. Chu, 1992. Equilibrium response of ocean deep-water circulation to variations in Ekman pumping and deep-water sources. J. Phys. Oceanogr., **22**, 1129-1157.